Testis dosimetry in individual patients by combining a small-scale dosimetry model and pharmacokinetic modeling-application of (111)In-Ibritumomab Tiuxetan (Zevalin(®)).

Meerkhan, Suaad; Sjögreen Gleisner, Katarina; Larsson, Erik; Strand, Sven-Erik; Jönsson, Bo-Anders

Published in:
Physics in Medicine and Biology

DOI:
10.1088/0031-9155/59/24/7889

2014

Testis dosimetry in individual patients by combining a small-scale dosimetry model and pharmacokinetic modeling – application of ^{111}In-Ibritumomab Tiuxetan (Zevalin®)

Suaad A. Meerkhan[1,2], Katarina Sjögreen-Gleisner[1], Erik Larsson[1], Sven-Erik Strand[1] and Bo-Anders Jönsson[1,*]

[1] Medical Radiation Physics, Department of Clinical Sciences, Lund, Lund University, SE-221 00 Lund, Sweden

[2] University of Duhok, Duhok, Iraq

* Corresponding author: Bo-Anders.Jonsson@med.lu.se

Running head: Testis small-scale dosimetry and compartment modeling

Journal template: Physics of Medicine and Biology

Abstract

A heterogeneous distribution of radionuclides emitting low-energy electrons in the testicles may result in a significant difference between an absorbed dose to the radiosensitive spermatogonia and the mean absorbed dose to the whole testis. This study focused on absorbed dose distribution in patients at a finer scale than normally available in clinical dosimetry, which was accomplished by combining a small-scale dosimetry model with patient pharmacokinetic data. The activity in the testes was measured and blood sampling was performed for patients that underwent pre-therapy imaging with ^{111}In-Zevalin®. Using compartment modeling, testicular activity was separated into two components: vascular and extravascular. The uncertainty of absorbed dose due to geometry variations between testicles was explored by an assumed activity micro-distribution and by varying the radius of the interstitial tubule. Results showed that the absorbed dose to germ cells might be strongly dependent on the location of the radioactive source, and may exceed the absorbed dose to the whole testis by as much as a factor of two. Small-scale dosimetry combined with compartmental analysis of clinical data proved useful for gauging tissue dosimetry and interpreting how intrinsic geometric variation influences the absorbed dose.

Keywords: small-scale dosimetry, compartment modeling, testicular uptake, ^{111}In-Zevalin

1. Introduction

The scale to which the absorbed dose can be determined from clinical nuclear medicine images is most often limited by the spatial resolution of the imaging system used. Due to low spatial resolution tissues may appear to have a homogenous activity distribution while the actual pattern of energy deposition remains quite heterogeneous. One methodology that can be applied to investigate absorbed dose distribution at a finer scale is to combine small-scale dosimetry models and patient pharmacokinetic data. A tissue where this is important and relevant is the testis. It is well known that the testis is a highly radiosensitive organ and considered a critical tissue in both diagnosis and therapy with ionizing radiation. The limit for deterministic effects, that is, temporary sterility, is only 150 mGy, while permanent sterility may occur at absorbed doses of 2 Gy y^{-1} or single exposures of 3.5–6 Gy (ICRP 1984). However, less is known about the occurrence of radiation-induced cancer in the testes (Yousif *et al* 2010), but any radiation-induced mutation in the germ cells that may cause genetic disease in humans has not been reported (BEIR 2006). However, in radiation protection and risk estimates, this cannot be disregarded and the ICRP has assigned a tissue weighting factor of 0.08 for the gonads (ICRP 2007).

One example in radioimmunotherapy where there is a potential risk of toxic effects on the gonads is the treatment for non-Hodgkin's lymphoma with ^{90}Y-Zevalin® (Spectrum Pharmaceuticals, Inc. USA). For instance, after a treatment male patients may experience temporary or permanent sterility, and according to EANM's guidelines, treatment of males of fertile age should be carried out with caution (Tennvall *et al* 2007). ^{90}Y-Zevalin® therapy is administered by an intravenous infusion (normally 15 MBq kg^{-1} with a maximum of 1.2 GBq), and absorbed dose values to the testis have been reported to fall between 2.2 and 9.1 mGy MBq^{-1} (Chiesa *et al* 2009; Cremonesi *et al* 2007; Fisher *et al* 2009; Shen *et al* 2005; Sjögreen-Gleisner *et al* 2011; Wiseman *et al* 2003a; Wiseman *et al* 2003b). Estimated mean absorbed doses to the testis from ^{111}In-Zevalin®, have been reported to fall between 0.2 and 2.4 mGy MBq^{-1} (Fisher *et al* 2009; Wiseman *et al* 2003b). Because the radionuclide ^{90}Y is a pure β^--emitter, imaging is considered difficult in clinical settings. Instead, imaging the biodistribution of ^{90}Y-Zevalin has generally been performed using ^{111}In-Zevalin as a surrogate, by the assumption that the

biological behavior of the two Zevalin-agents is identical (Sjögreen-Gleisner *et al* 2011). Likewise, the majority of reported dosimetry studies are based on ^{111}In-Zevalin imaging. In some cases, an ^{111}In-Zevalin study has been used for planning the absorbed dose of a subsequent ^{90}Y-Zevalin treatment (Sjögreen-Gleisner *et al* 2011).

The absorbed doses reported above refer to the average absorbed dose to the whole testis, which according to conventional MIRD dosimetry assumes a homogenous activity distribution within the organ (Bolch *et al* 2009). However, the absorbed dose to the regions with radiosensitive germ cells may be significantly higher, or lower, depending on the true activity distribution, which is likely to be non-homogenous among different testicular compartments. For instance, it has previously been shown in multilevel autoradiography studies that ^{111}In-transferrin is highly non-homogeneously localized in the testis. The uptake was reported to be mainly localized in the interstitial tissue, but with an uptake in the spermatogonial region well above the average level (Jönsson *et al* 1992b; Jönsson *et al* 1992c). It is well known that germ cells have different radiation sensitivities, with the highest for undifferentiated spermatogonia near the basal cell layer. The more mature sperm cells migrating toward the lumen have the lowest sensitivity (Centola *et al* 1994; Meistrich 1986). Hoyes et al. (1994) demonstrated that activity localization in the intratesticular tissue may result in spermatogenic damage (Hoyes *et al* 1994) and that human spermatozoa in vitro appears to accumulate transferrin-binding metals such as ^{111}In (Hoyes *et al* 1998). Some radiometal-based radiopharmaceuticals have also been reported to be retained in the testicular tissue (Jackson *et al* 1991; Jönsson *et al* 1992a; Nettleton *et al* 2004; Rao *et al* 1983). However, their precise localization is unknown and remains to be determined. Another source region that may contribute significantly to the absorbed dose to the sensitive germ cells is circulating plasma-bound activity, which is localized in the vasculature of the interstitial tissue.

A need has been established for developing more detailed dosimetry models based on tissue structures in internal dosimetry (Howell *et al* 2006; ICRU 2002; Sgouros *et al* 2009). Our group recently published a small-scale dosimetry model developed for detailed testis dosimetry (Larsson *et al* 2012).

This model permits the calculation of the absorbed dose to different target cells in the testicular tissue from radionuclides used in nuclear medicine, with a choice of source regions (i.e., the interstitial tissue and the different cell layers in the seminiferous tubules). The latter corresponds to the sites of spermatogenesis, the complex process where germ cells proliferate and transform into spermatozoa. The aim of the present study was to calculate the absorbed dose to the spermatogonia region for ^{111}In Zevalin®, based on the new small-scale dosimetry model and the S-values calculated therein, assuming a hypothetical but realistic activity micro-distribution. The biokinetics were obtained from blood sampling and whole-body imaging of four patients, along with subsequent image-based quantification of whole-testes activity. To refine and resolve the small-scale distribution activity, a compartmental model was used for separating the activity into vascular and extravascular compartments; this was solved by combining image-based activity estimates with blood sampling (Nickel *et al* 2009; Sjögreen-Gleisner *et al* 2007).

2. Material and Methods

2.1 Patient data

Data from four patients were included, referred for pre-therapy imaging with ^{111}In-Zevalin® (Spectrum Pharmaceuticals, NV, USA) for absorbed dose planning prior to RIT of B-cell lymphoma with ^{90}Y-Zevalin® (Spectrum Pharmaceuticals, NV, USA). The patients were intravenously injected with 290–300 MBq ^{111}In-Zevalin® (table 3). Whole-body planar imaging was performed at seven points: 1, 24, 48, 72, 144, 166, and 192 h after injection. A dual-head Discovery SPECT/CT VH system (General Electric, Milwaukee, WI) was used for image acquisition. Anterior and posterior whole-body images were acquired using a 15% energy window centered over the 245-keV photopeak, employing medium-energy general-purpose collimators. For the purpose of attenuation correction, a whole-body planar transmission image (X-ray scout image) was acquired at 24 h. For quantification of the ^{111}In-Zevalin® distribution, images were exported in the DICOM image format to an independent computer platform for further processing in the LundADose software (Sjögreen *et al* 2005). In brief, the activity quantification included several steps: a) explicit correction for scatter in the anterior–posterior whole-

body images by deconvolution (Sjögreen-Gleisner 2012); b) calculation of a geometric mean image by pixel-by-pixel multiplication of scatter-corrected anterior and mirrored posterior projections; and c) pixel-based attenuation correction using a co-registered whole-body attenuation map calculated from the X-ray scout image (Sjögreen-Gleisner and Ljungberg 2012). The image obtained from these steps was a count-rate projection without effects of attenuation or scatter, i.e. as if the activity were situated in air, and could thus be converted to an activity projection using a measured value of the system sensitivity in air (cps MBq^{-1}) for ^{111}In. Note that this procedure did not use the amount of injected activity for calibration, and thus represented an independent quantification of the activity distribution in the patient. By careful manual delineation of regions of interest (ROI) over the testes region in the images at each point in time, the regional activity was quantified using the image processing program ImageJ (Research Services Branch, National Institute of Mental Health, Bethesda, Maryland, USA). Blood samples were collected at 5 and 45 min and at 3, 6, 24, 48, 72, 144, 168 and 190 h after administration. Plasma was centrifuged for separation, weighed, and the activity was measured in a calibrated well-type NaI(Tl) detector (1282 CompuGamma CS; Wallac).

2.2 Compartmental modeling

Total activity in the testis was divided into a vascular and an extravascular part by compartmental analysis (Nickel *et al* 2009; Sjögreen-Gleisner *et al* 2007). The model used is shown in figure 1.

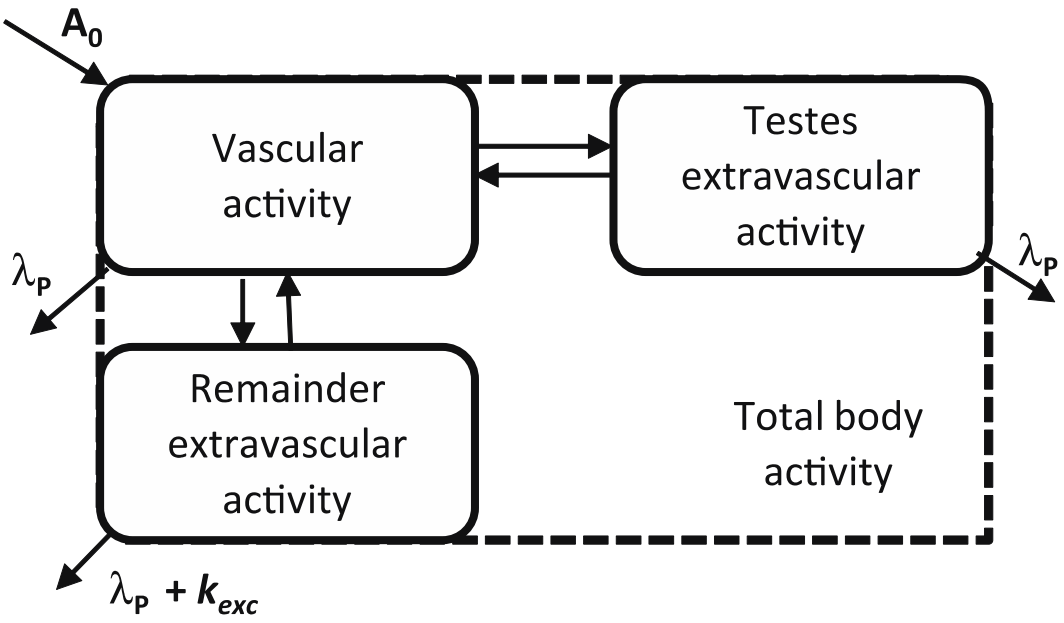

Figure 1. The compartment model used for pharmacokinetic modeling, where A_0 was the administered activity, λ_p the rate of physical decay, and k_{exc} the rate constant of excretion.

The total activity in the testes at time *t*, $A^{tes}(t)$, was described as

$$A^{tes}(t) = A_v^{tes}(t) + A_{ev}^{tes}(t) \quad (1)$$

where $A_v^{tes}(t)$ and $A_{ev}^{tes}(t)$ are the activities (MBq) within the vascular and extravascular spaces of the testes. The curve $A^{tes}(t)$ was determined as part of model optimization by minimizing its deviation from the measured testes activity values. The curve $A_v^{tes}(t)$ was described as the vascular activity in total body, $A_v^{tb}(t)$, multiplied by a regional vascular fraction, ϕ, denoting the fraction of the total-body vascular volume contained in testes:

$$A_v^{tes}(t) = \phi\, A_v^{tb}(t) \quad (2)$$

The curve $A_v^{tb}(t)$ was described as

$$A_v^{tb}(t) = \begin{cases} C_{pl}(t) \cdot V_{pl} \cdot \rho_{pl} \\ C_{bl}(t) \cdot V_{bl} \cdot \rho_{bl} \end{cases} \quad (3)$$

where $C_{pl}(t)$and $C_{bl}(t)$ (MBq/g) denote activity concentrations, V_{pl} and V_{bl} are total-body volumes (mL), and ρ_{pl} and ρ_{bl} (g/mL) denote mass densities, of plasma and whole blood, respectively. Values

of ρ_{pl} and ρ_{bl} were set to 1.03 g/mL and 1.06 g/mL, respectively (ICRP 2002). For optimization of the curve $A_v^{tb}(t)$ measured values of activity concentrations in plasma and whole blood were used. Moreover, the injected activity, A_{inj}, was modeled as a bolus at time zero with a value equating the administered amount for the patient, which in equation 3 introduced the constraint that $A_v^{tb}(0)$ should equal A_{inj}. The disappearance of activity from blood was due to extravasation and uptake in different tissues and organs. To simplify the analysis, the model for extravascular activity was limited to the testes and a remainder compartment. The activity in total body, $A^{tb}(t)$, was thus modeled as the sum

$$A^{tb}(t) = A_v^{tb}(t) + A_{ev}^{tes}(t) + A_{ev}^{rem}(t) \tag{4}$$

The curve $A^{tb}(t)$ was determined as part of model optimization by minimizing its deviation from measured values of total-body activity from image-based quantification. Moreover, at the time of administration the values of $A_{ev}^{rem}(0)$ and $A_{ev}^{tes}(0)$ were equal to zero, thus implying that $A^{tb}(0)$ should equal $A_v^{tb}(0)$, which introduced further constraints for the free parameters V_{pl} and V_{bl} in equation 3. The activities in the extravascular compartments were determined by solving the linear differential equations

$$\frac{dA_v^{tb}(t)}{dt} = -\left(k_{tes\leftarrow v} + k_{rem\leftarrow v} + \lambda_p\right)A_v^{tb}(t) + k_{v\leftarrow tes}A_{ev}^{tes}(t) + k_{v\leftarrow rem}A_{ev}^{rem}(t) \tag{5}$$

$$\frac{dA_{ev}^{tes}(t)}{dt} = k_{tes\leftarrow v}A_v^{tb}(t) - \left(k_{v\leftarrow tes} + \lambda_p\right)A_{ev}^{tes}(t) \tag{6}$$

$$\frac{dA_{ev}^{rem}(t)}{dt} = k_{rem\leftarrow v}\,A_v^{tb}(t) - \left(k_{v\leftarrow rem} + k_{exc\leftarrow rem} + \lambda_p\right)A_{ev}^{rem}(t) \tag{7}$$

where the *k* parameters are rate constants with *v*, *tes*, *rem*, *exc* denoting compartments vascular, testes, remainder, and excretion, respectively, and λ_p is the rate of physical decay (h^{-1}). This model was implemented in SAAM II (The Epsilon Group, VA, USA), which is a commercial software package that supports compartmental modelling through a graphical user interface. The model was solved

using a Cash-Karp variant of the embedded Runge-Kutta method (Press *et al* 1992) and assuming data variance described by Poisson statistics. The cumulated activities of the testes compartments, i.e. total, vascular, extravascular, and the associated uncertainties, were calculated by numerical integration. An integration time of 1000 h was chosen so that no further increase in the cumulated activities occurred. The fraction of cumulated activity in the respective compartments was then determined, with its uncertainty estimated by error propagation.

2.3 Calculation of the absorbed dose

The absorbed dose to the spermatogonia (the most radiosensitive cells in the testis) was calculated using the recently published S-values from the small-scale dosimetry model by Larsson et al. (Larsson *et al* 2012). Briefly, the geometry of the model consists of a hexagonal pattern of 250-μm diameter cylinders, representing the seminiferous tubules, with a 10-μm space between tubules corresponding to the interstitial tissue. Each seminiferous tubule was divided into nine concentric cylinders, equal to the different germ cell layers, starting at the basement membrane with the very radiosensitive spermatogonia then extending toward the lumen, where the less radiosensitive mature spermatids are migrating to the epididymis. The geometry was modeled in the MCNP5 1.4 Monte Carlo-code package (Los Alamos, NM, USA) as described in Larsson et al., and absorbed fractions were derived for monoenergetic particles and S-values for different radionuclides.

It has been reported in the literature that the diameter of the seminiferous tubule varies between 150 and 300 μm (Holstein *et al* 2003; ICRP 2002). In order to investigate the uncertainty originating from the unpredictable geometry of the testis, the previously fixed size of the seminiferous tubule radii was varied between 100 and 200 μm. Since the diameter of the male germ cells of different stages as well as the extension of their cell layers are considered to be relatively equal, the layer thickness seen from the basement membrane was kept fixed, only allowing change in the lumen thickness. Monte Carlo simulations (MCNP5 1.51, Los Alamos, NM: Los Alamos National Laboratory) of energy deposition were then carried out with this modified geometry to calculate new S-values. The number of particles

simulated was set to get a statistical uncertainty below 1%. Although the original model allows one to choose several optional source-target regions within the testis tissue, only three source regions were selected in the present study, in order to characterize a hypothetical but realistic uptake of radioactivity in the i) interstitial tissue, ii) spermatogonia, and iii) lumen (see figure 2). The uptake in the interstitial tissue may then represent the most probable case whereas an uptake by spermatogonia represent a worst case situation..

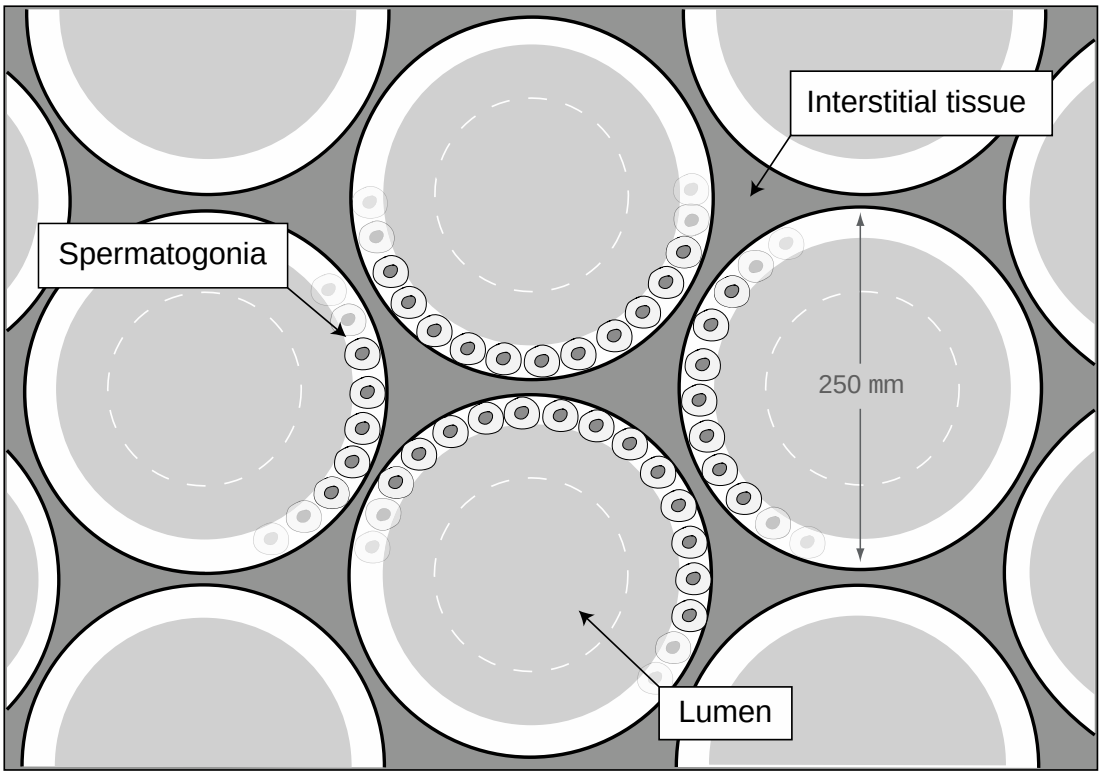

Figure 2. Cross-section showing the three different sources used in this the dosimetry study: interstitial tissue, spermatogonia and lumen.

The S-values generated for calculation are presented in table 1. The decay data of ^{111}In were retrieved from the Radiation Decay 3 software package (Charles Hacker, Griffith University, Gold Coast, Australia), which is based on data from the Radiation Shielding Information Center at Oak Ridge National Laboratories (TN, USA). These data are summarized in table 2.

Table 1a. S-values ($mGyMBq^{-1}s^{-1}$) for ^{111}In according to (Larsson *et al* 2012)[a].

Target	Source		
	Interstitial tissue	Spermatogonia	Lumen
Interstitial tissue	1.02E-03	5.45E-04	5.10E-04
Spermatogonia	5.50E-04	1.10E-03	5.07E-04
Lumen	5.15E-04	5.12E-04	1.03E-03

[a] $S_{testes \leftarrow testes}$ (^{111}In) = 6.10E-4 $mGyMBq^{-1}s^{-1}$

Table 1b. S-values ($mGyMBq^{-1}s^{-1}$) for ^{90}Y according to (Larsson *et al* 2012)[a].

Target	Source		
	Interstitial tissue	Spermatogonia	Lumen
Interstitial tissue	9.49E-03	9.33E-03	9.18E-03
Spermatogonia	9.46E-03	9.71E-03	8.95E-03
Lumen	8.97E−03	9.39E−03	9.97E-03

[a] $S_{testes \leftarrow testes}$ (^{90}Y) = 9.24E-3 $mGyMBq^{-1}s^{-1}$

Different fractions of activity between the regions were assumed to represent the most likely case (i.e., all activity localized in the interstitial tissue) to the worst case (i.e., all activity in the region of spermatogonia). The model was developed for the microstructure of the testicular tissue, but still follows the well-established MIRD formula (Bolch *et al* 2009):

$$D_{r_T} = \sum_{r_S} \frac{\tilde{A}_{r_S} \Delta \phi\left(r_T \leftarrow r_S\right)}{m_{r_T}} = \sum_{r_S} \tilde{A} \cdot S\left(r_T \leftarrow r_S\right) \tag{8}$$

where D_{r_T} is the absorbed dose to a target region r_T, and $\tilde{A}_{r_S}$ is the cumulated activity in source region r_S. The Δ is the mean energy emitted per nuclear transformation from the source and $\phi\left(r_T \leftarrow r_S\right)$ is the fraction of the radiation energy emitted from the source region, r_T, that is absorbed in the target region, r_S. The product of the quantities Δ and $\phi\left(r_T \leftarrow r_S\right)$ divided by m_{r_T}, the mass of the target region, is designated by the S-value, which is radionuclide- and anatomy-specific.

Table 2. Average energy of emitted energy from ^{111}In with corresponding electron ranges in water

Radiations	Average energy (keV)	Yield	CSDA-range[a] (μm)
Conversion electrons			
KLM, γ_1	147.76	0.098	275
KLM, γ_2	222.52	0.060	534
Auger electrons			
KXY	19.63	0.154	8
LXY	2.66	1.015	< 0.3
Photons			
γ_1	171.30	0.906	
γ_2	245.40	0.941	
$K_{\alpha,\beta}$ X-rays	23.58	0.680	

[a] Continuous-slowing-down approximation, i.e. the average path length traveled by a charged particle as it slows down to rest (ICRU 1984).

3 Results

3.1 Biokinetics and Compartment Analysis

The results for the compartment analysis of the biokinetic data of testes from the individual patients are given in figure 3 and table 3. To enable comparison of model-derived curves of the activity in plasma and whole blood in testes, the measured values of the activity concentrations have been multiplied by the factors $(\phi \cdot V_{pl} \cdot \rho_{pl})$ and $(\phi \cdot V_{bl} \cdot \rho_{bl})$, for plasma and whole blood, respectively. The regional vascular fraction in the testes, i.e. the fraction of administered activity (extrapolated to the time of administration), ranged from 0.37% to 0.70% for the four patients. Initially all activity is in the vascular space, but the extravascular activity increases during the first two days and equals the vascular activity at 38−68 h after injection. A secular equilibrium is then established and the extravascular activity decreases approximately at the same rate as the vascular component. The fraction of each component of the area under the curve, that is the cumulated activity ($\tilde{A}$), varies between individuals as can be seen in table 3.

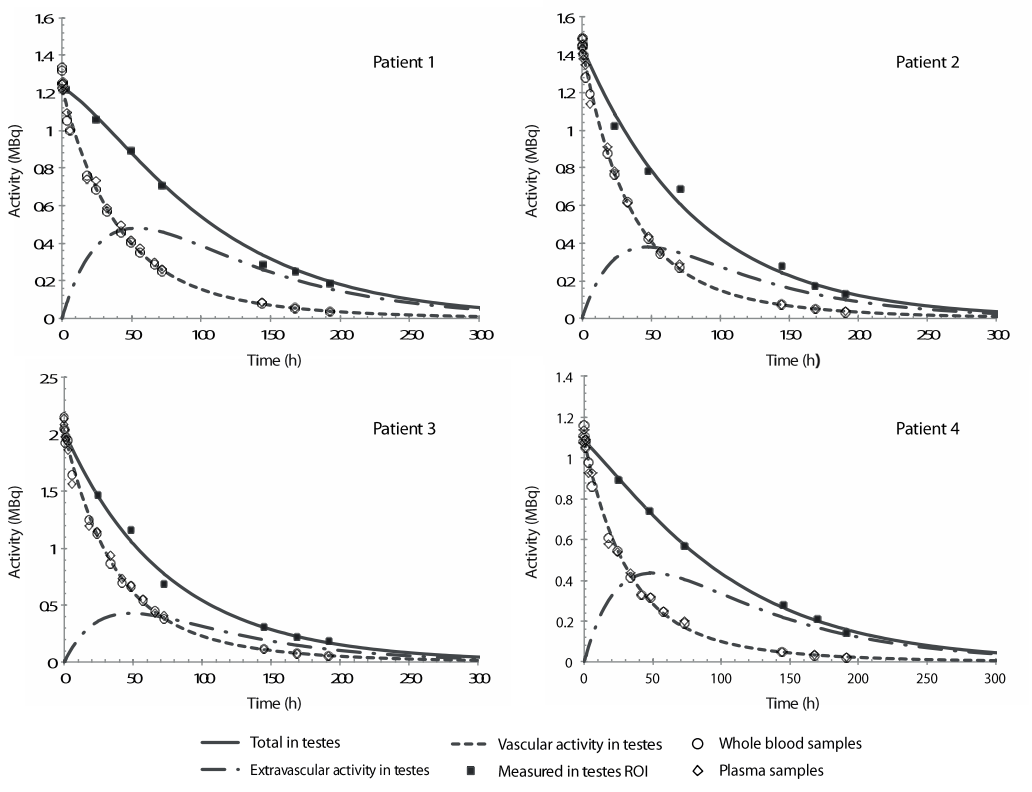

Figure 3. Time-activity curves obtained for the testis ROI as quantified from planar scintillation camera images for the four patients included in the study. The solid box markers represent the measured activity, the open symbols represent the activity in plasma (diamonds) and whole blood (circles) contained in testes (see text), solid line is the fitted total-activity curve, the short dashed line is the vascular activity, and the dot-dashed line is the extravascular activity. The time when the tissue activity equals the activity in the blood vessels varies between 40 and 79 h for the four patients.

Table 3. Measured and calculated parameters for the dosimetry of ^{111}In-Zevalin® in the testes for the four patients.

Patient	Administered activity (MBq)	Regional vascular fraction (%)	$\tilde{A}$ (MBq h)	Fraction of $\tilde{A}$	
				Vascular	Extravascular
1	298	0.41	137 ±3	0.44 ±0.02	0.56 ±0.03
2	297	0.49	118 ±4	0.53 ±0.03	0.47 ±0.04
3	290	0.70	155 ±5	0.60 ±0.03	0.40 ±0.04
4	300	0.36	112 ±2	0.40 ±0.01	0.60 ±0.02

A representative result of activity in total body and in vascular spaces for patient 2 is shown in figure 4. In similar to results in Figure 3, comparison of model-derived curves of the activity in plasma and whole blood in total body was achieved by scaling the measured values of the activity concentrations by the factors $(V_{pl} \cdot \rho_{pl})$ and $(V_{bl} \cdot \rho_{bl})$, for plasma and whole blood, respectively. As seen, curves obtained from compartment modeling fit measured data very well, and equally good fits were obtained for the other patients. The total-body blood volumes were obtained to 4830±76 mL, 5144±41 mL, 5738±65 mL, and 4833±65 mL (±1 standard deviation), for patients 1-4, respectively, and plasma volumes obtained were 3292±41 mL, 3452±33 mL, 3632±49 mL, and 3010±46 mL, for patients 1-4, respectively. The standard deviations obtained were thus between 0.81% and 1.58% of the determined values. Values obtained compare well with population reference values of 5300 mL and 3000 mL, for whole blood and plasma volumes, respectively (ICRP 2002).

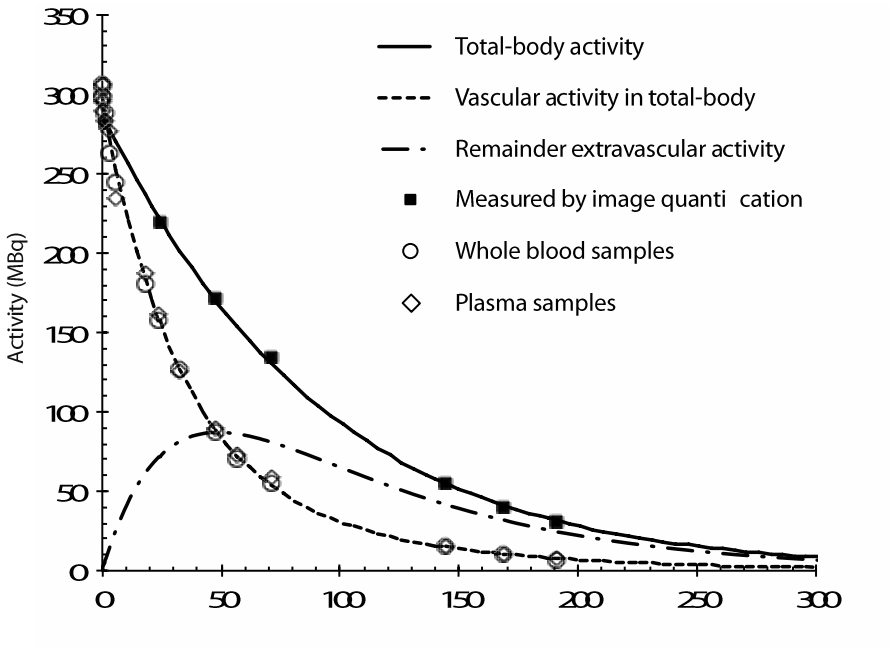

Figure 4. Time-activity curves for total body for patient 2. Solid box markers represent the quantified total-body activity from scintillation camera images. Open symbols represent the activity in plasma (diamonds) and whole blood (circles) contained in total body (see text), solid line is the fitted total-activity curve, the short dashed line is the vascular activity, and the dot-dashed line is the extravascular activity. Model-derived curves fit measured data well, and results for the other patients were equally good.

3.2 Absorbed dose calculation

The absorbed dose to the testis was calculated individually for the four patients according to their biokinetic data (table 3) for the three cases of activity distribution. These are given in table 4A–C. In case 1, the absorbed dose to the target regions is calculated assuming that 100% of the testis activity is localized homogenously in both the vascular and the extravascular space in the interstitial tissue (IT). In this case no activity has penetrated the blood–testes barrier, and all exposure of the cells in the seminiferous tubules originates from radiation emitted in the interstitial tissue. In case 2, based on the compartment analysis, around half of the decays are in the vascular space and half in the peripheral region of the tubule, i.e. the site of the radiosensitive spermatogonia, see table 4 for individual values.

Finally, case 3 exemplifies when the activity in the tubule is localized more centrally, i.e. in the lumen containing radio-resistant sperm. The absorbed doses in each region are compared to the mean absorbed dose to the whole testis.

As expected, the source region receives the highest absorbed dose due to the self-dose from low energy conversion and Auger electrons (see table 2). It is interesting to note that when the IT accounts for all activity, the adjacent spermatogonial region may receive an absorbed dose that is 11% lower than the mean absorbed dose to the whole testis, i.e. 0.44 and 0.49 mGy MBq^{-1}, respectively (case 1; table 4). However, if 50% of the activity is localized in the spermatogonial region, the absorbed dose to the early germ cells (spermatogonia and spermatocytes) will be 37% greater than the whole testis absorbed dose (case 2; table 4). However, if the 50% activity fraction is localized in the luminal space (spermatids and spermatozoa), the absorbed dose to the spermatogonia decreases to 17% of the mean absorbed dose and 66 % of the absorbed dose to the spermatozoa. The IT itself will in all cases receive an absorbed dose greater than the whole testis absorbed dose by 20–65%.

Table 4. Absorbed dose from ^{111}In-Zevalin in each target region: interstitial tissue, spermatogonia, and lumen for the three cases of activity distribution studied. Each absorbed dose was calculated individually for the four patients and compared to the average absorbed dose to the whole testis.

A. Case 1. Source: 100% localized in interstitial tissue (vascular + extravascular)

Patient	Absorbed dose (mGy MBq^{-1})			
	Interstitial tissue	Spermatogonia	Lumen	Whole testis
1	0.85	0.46	0.43	0.51
2	0.73	0.39	0.37	0.44
3	0.98	0.53	0.50	0.59
4	0.69	0.37	0.35	0.42
Mean	0.81	0.44	0.41	0.49

B. Case 2. Source: X% localized in interstitial tissue (vascular) and Y% in the spermatogonial region (extravascular)

Patient	Absorbed dose (mGy MBq^{-1})			
(X:Y)	Interstitial tissue	Spermatogonia	Lumen	Whole testis
1 (44:56)	0.63	0.71	0.43	0.51
2 (53:47)	0.57	0.58	0.37	0.44
3 (40:60)	0.80	0.74	0.49	0.59
4 (60:40)	0.49	0.59	0.34	0.42
Mean (49:51)	0.61	0.67	0.41	0.49

C. Case 3. Source: X% localized in interstitial tissue (vascular) and Y% in the luminal region (extravascular)

Patient	Absorbed dose (mGy MBq^{-1})			
	Interstitial tissue	Spermatogonia	Lumen	Whole testis
1 (44:56)	0.61	0.44	0.67	0.51
2 (53:47)	0.56	0.38	0.54	0.44
3 (40:60)	0.78	0.51	0.69	0.59
4 (60:40)	0.48	0.35	0.55	0.42
Mean (49:51)	0.59	0.42	0.63	0.49

3.3 Uncertainty due to geometry variations

In the cases above, a fixed diameter of 250 μm was used for the seminiferous tubule, according to our published model (Larsson *et al* 2012), To relate influence of the geometry on the absorbed dose profile to our three cases, the radius of the seminiferous tubule was varied between 100 and 200 μm. The results of the simulation of modified S-values with this slightly altered geometry are presented in figure 5, which shows the ratio between the absorbed dose to respective target regions and the mean absorbed dose to the whole testis for the three cases. Hence, the source is either the interstitial tissue (e.g. blood vessels, macrophages, and Leydig cells), the spermatogonium (spermatogonia) or the lumen (mature spermatids), and the absorbed dose ratio profiles are shown throughout the seminiferous tubule starting from the basement membrane (lamina propria).

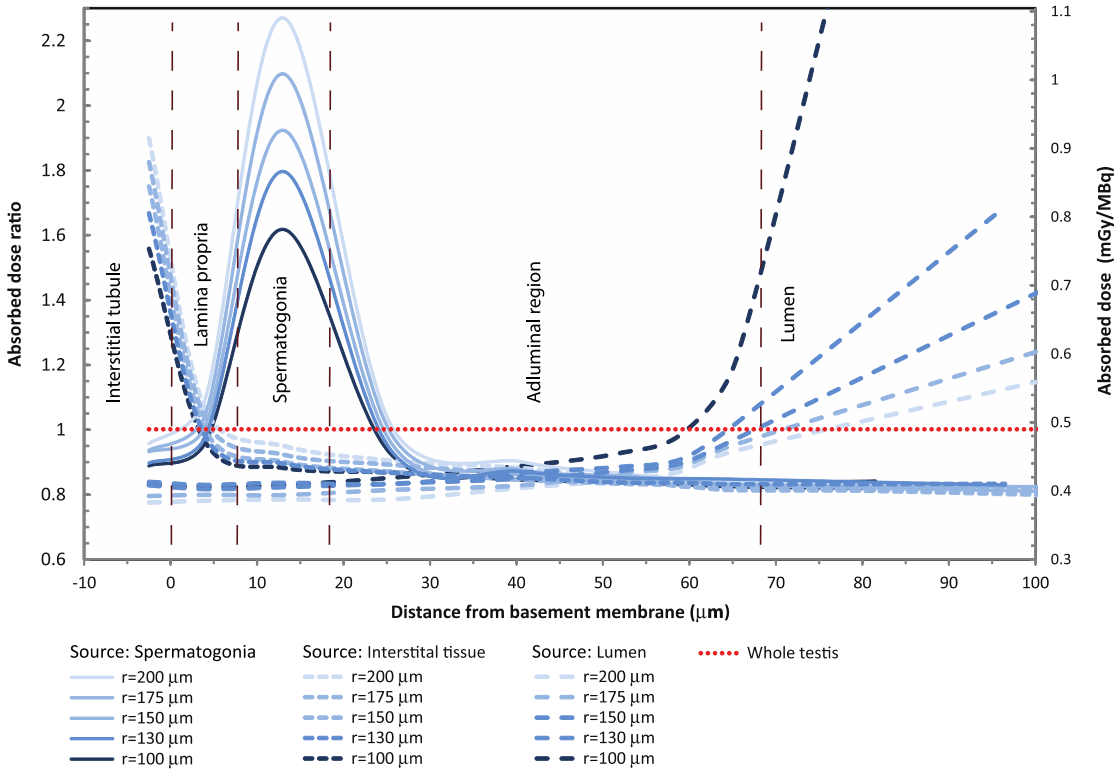

Figure 5. The ratio between the absorbed dose for ^{111}In in different layers of the seminiferous tubule and the whole testis, for seminiferous tubule radius varying from 100 to 200 μm. The source activity was either in interstitial tissue, spermatogonia, or lumen. Correspondingly, the absorbed dose per administered activity in mGy MBq^{-1} is shown on the right axis. The dotted line represents the case of homogeneous activity distribution in testis, with absorbed dose ratio being unity and an average absorbed dose of 0.49 mGy MBq^{-1}.

The calculations show the spermatogonia ^{111}In self-dose to whole-testis absorbed dose ratio increasing from 1.61 to 2.27 (26%) as the seminiferous tubule radius is enlarged from 100 to 200 μm. This is mainly due to the changes in weight, but a 15% reduction in the absorbed fraction is observed as well. The cross-dose from other regions to the spermatogonia also changes as the radii of the seminiferous tubules are varied, due to the increased distance between them. The absorbed dose ratio from IT to spermatogonia is increased from 0.89 to 0.95, whereas the absorbed dose ratio from lumen to

spermatogonia is decreased from 0.83 to 0.79. Using the biokinetic data from the patients, the absorbed dose in mGy per MBq administered activity is presented concurrently and can be read on the right axis in figure 5.

4. Discussion

The testis is considered a critical tissue in both diagnosis and therapy with ionizing radiation, with very low absorbed dose limits for both temporary and permanent sterility. For external exposure, it is relatively simple to measure and determine the absorbed dose to a critical organ, and different precautions have been developed to protect organs at risk. However, the precautions for diagnostic X-ray examinations (e.g., scrotum-capsule shields) and external radiotherapy (e.g., field techniques and shaping) are in principle impossible to use in nuclear medicine procedures. On the other hand, the accuracy of internal dosimetry has been considerably improved since the introduction of the MIRD methodology (Loevinger and Berman 1976) for making dose estimations to predict possible organs at risk. Discussions on dosimetry often concern uncertainty in the determination of the absorbed dose and the relevance to possible stochastic or deterministic damages. In nuclear medicine, the main concern has so far been stochastic (long-term) effects, but the increasing use of very high activities in radionuclide therapy now also include concerns over deterministic effects to critical organs, such as bone marrow, intestines, kidneys and gonads. One main obstacle in conventional dosimetry is the lack of knowledge of detailed activity localization within the tissue, and the activity is therefore simply assumed to be homogenously distributed throughout the organ. This assumption is mostly based on activity biokinetic data obtained from SPECT/PET imaging with insufficient spatial resolution for accurate dosimetry. In this work planar imaging and was used for quantification of the activity in testes. We recognize that, generally, SPECT imaging is regarded a superior technique for activity quantification mainly due to superimposing activity in overlapping structures seen in planar images. However, this problem was not so apparent for the testes, being a body region, which is less overlapped by other structures. Moreover, the testes are rarely covered by the SPECT field-of-view, as was the case for the patients included in this study. Owing to the small extension of the testes

compared to other body regions it was considered important to make explicit attenuation correction, and was achieved using a pixel-based quantification scheme where an X-ray scout image is used as attenuation correction map. The internal dosimetry community continuously discusses the necessity for improvements to bring about more detailed tissue and cellular dosimetry (Hobbs *et al* 2012; Howell *et al* 2006; ICRU 2002; Sgouros and Hobbs 2014; Sgouros *et al* 2009). One direction has been the development of detailed small-scale dosimetry models but the practical use is so far unfortunately limited due to the difficulties in determining detailed activity localization for the tissue in question. However, small-scale dosimetry models can serve as an essential bridge between macroscopic and cellular dosimetry. For instance, such models may act as an indicator of uncertainties arising from intrinsic geometry variation at tissue level, and are especially relevant to investigating the influence of the energy absorption pattern of low-energy electrons and soft X-rays. The original MIRD-formalism introduced the concepts of penetrating and non-penetrating radiation for photons and charged particles, respectively. While the absorbed fraction $\phi(r_T \leftarrow r_S)$ for photons varies between 0 and 1, charged particles such as electrons have $\phi(r_T \leftarrow r_S) = 1$ if $r_T = r_S$ (i.e. the source and target are the same) and $\phi(r_T \leftarrow r_S) = 0$ if $r_T \neq r_S$. However, with the development of small-scale anatomical models and emitted particles whose range in tissue is short relative to the dimensions of the target regions, the boundary between penetrating and non-penetrating radiation is vague, and small-scale anatomic model model-based calculations are necessary in these cases. This has been clearly shown by a number of authors (Goddu *et al* 1993; Hobbs *et al* 2011; Jönsson *et al* 2002; Larsson *et al* 2005; Larsson *et al* 2012; Sgouros and Hobbs 2014; Stenvall *et al* 2014). The present paper focus on the testicular tissue and presents how the small-scale dosimetry model by Larsson et al. (Larsson *et al* 2012) could be combined with compartmental modeling based on pre-therapy data (i.e., serial quantitative scintillation camera images and blood sampling) from patients in order to separate the activity retained in the testis into extravascular and vascular components (Nickel *et al* 2009). This novel approach may be valuable in cases where the exact tissue localization of the activity is unknown but recognized to be taken up in the tissue (extravascular component) with a longer retention time than in the blood (vascular component).

The three cases studied in this work are hypothetical but have support in the literature—for instance, the most probable site of radiopharmaceutical localization is the interstitial tissue. This is because the blood–testis barrier consists of the Sertoli cells, which efficiently inhibit harmful agents from entering the seminiferous epithelium (Bart *et al* 2002). However, ^{111}In and some other radiometals have been reported to traverse the blood–testis barrier, probably by utilizing the iron-transferrin pathway, to accumulate inside the seminiferous epithelium (Hoyes *et al* 1996; Hoyes *et al* 1998; Hoyes *et al* 1994; Jönsson *et al* 1992b; Nettleton *et al* 2004).

Based on biological pre-therapy patient data, the macroscopic dosimetry resulted in absorbed doses to the whole testis of 0.5 mGy MBq^{-1} from ^{111}In-Zevalin©, which is the same level as reported previously (Shen *et al* 2005; Wiseman *et al* 2003a). However, although the detailed localization of ^{111}In-Zevalin© in the patient testis is not yet known and remains to be explored, it is obvious from the present small-scale dosimetry model that the absorbed dose is highly dependent of the site of activity localization and on natural geometric variations of the interstitial tubules. As a worst case, i.e. the basal compartment as the source, the absorbed dose to spermatogonia might exceed the whole testis mean absorbed dose by a factor of 1.6–2.3, depending on the radius of the seminiferous tubule. On the other hand, if no activity at all passes the blood–testis barrier, i.e. all activity is localized in the interstitial tissue, the absorbed dose to the spermagonia is about 10 % below the mean absorbed dose to the whole testis. Still, precautions have to be taken since even a diagnostic activity may reach the limit for deterministic temporary effects and enhanced risk for stochastic effects.

It can be seen that the average absorbed dose to the whole testis is 0.49 mGy MBq^{-1} or approximately 150 mGy if 300 MBq ^{111}In-Zevalin© is administered, consequently hitting the limit of absorbed dose and causing temporary sterility. Unlike for ^{111}In, a heterogeneous localization of ^{90}Y in the testis is not critical for the absorbed dose due to its long-range beta particles, and the absorbed dose will then be nearly the same throughout the testis, no matter the activity localization in different testicular compartments. The minor differences in S-values can be seen in table 1b. Thus, with the same

biokinetics as ^{111}In-Zevalin©, the absorbed dose from the ^{90}Y-Zevalin© should yield an average absorbed dose of 3.30 mGy MBq^{-1}. A treatment with the recommended therapy activity (i.e. 11.1 MBq kg^{-1} or a maximum of 1200 MBq) should then result in a testis absorbed dose of about 4 Gy (Larsson *et al* 2012) and undoubtedly result in permanent sterility. As a consequence, caution is recommended for the treatment of young male patients and semen cryopreservation may be appropriate prior to treatment (Tennvall *et al* 2007).

5. Conclusion

Small-scale dosimetry models combined with clinical patient biokinetics and compartment modeling may potentially serve as a bridge between organ and tissue dosimetry, and the interpretation of intrinsic geometric variation and its uncertainties in absorbed dose. In this paper, we focused on the dosimetry for the testicle and presented significant differences in the absorbed dose to the radiosensitive germ cells depending on the location of the radioactive source region and geometry variations of the seminiferous tubule.

Acknowledgements

The authors would like to acknowledge Jan Tenvall (M.D., Ph.D.) and Ola Lindén (M.D., Ph.D.), Department of Oncology, Skåne University Hospital – Lund, for the access to clinical data. This work was supported by the Swedish Radiation Safety Authority (grant 2010/4362); the Berta Kamprad Foundation (grant BKS 22/2013, and the Swedish Cancer Foundation (grant 120821).

References

Bart J, Groen H J M, van der Graaf W T A, Hollema H, Hendrikse N H, Vaalburg W, Sleijfer D T and de Vries E G E 2002 An oncological view on the blood–testis barrier *The Lancet Oncology* **3** 357-63

BEIR 2006 Health Risks from Exposure to Low Levels of Ionizing Radiation - BEIR VII Phase 2. ed N R Council (Washington DC

Bolch W E, Eckerman K F, Sgouros G and Thomas S R 2009 MIRD Pamphlet No. 21: A Generalized Schema for Radiopharmaceutical Dosimetry-Standardization of Nomenclature *Journal of Nuclear Medicine* **50** 477-84

Centola G M, Keller J W, Henzler M and Rubin P 1994 Effect of low-dose testicular irradiation on sperm count and fertility in patients with testicular seminoma *J Androl* **15** 608-13

Chiesa C, Botta F, Coliva A, Maccauro M, Devizzi L, Guidetti A, Carlo-Stella C, Seregni E, Gianni M A and Bombardieri E 2009 Absorbed dose and biologically effective dose in patients with high-risk non-Hodgkin's lymphoma treated with high-activity myeloablative 90Y-ibritumomab tiuxetan (Zevalin) *Eur J Nucl Med Mol Imaging* **36** 1745-57

Cremonesi M, Ferrari M, Grana C M, Vanazzi A, Stabin M, Bartolomei M, Papi S, Prisco G, Martinelli G, Paganelli G and Ferrucci P F 2007 High-dose radioimmunotherapy with Y-90-ibritumomab tiuxetan: Comparative dosimetric study for tailored treatment *Journal of Nuclear Medicine* **48** 1871-9

Fisher D R, Shen S and Meredith R F 2009 MIRD dose estimate report No. 20: radiation absorbed-dose estimates for 111In- and 90Y-ibritumomab tiuxetan *J Nucl Med* **50** 644-52

Goddu M S, Howell R W and Rao D V 1993 Cellular Dosimetry: Abosrbed fractions for monenergetic electron (0.1 keV - 1 MeV) and alpha particles (3 - 10 MeV) sources, and S-values for radionuclides, distributed uniformly in different cell compartments *Journal of Nuclear Medicine*

Hobbs R F, Baechler S, Fu D X, Esaias C, Pomper M G, Ambinder R F and Sgouros G 2011 A model of cellular dosimetry for macroscopic tumors in radiopharmaceutical therapy *Medical Physics* **38** 2892-903

Hobbs R F, Song H, Huso D L, Sundel M H and Sgouros G 2012 A nephron-based model of the kidneys for macro-to-micro alpha-particle dosimetry *Physics in Medicine and Biology* **57** 4403-24

Holstein A F, Schulze W and Davidoff M 2003 Understanding spermatogenesis is a prerequisite for treatment *Reprod Biol Endocrinol* **1** 107

Howell R W, Neti P V, Pinto M, Gerashchenko B I, Narra V R and Azzam E I 2006 Challenges and progress in predicting biological responses to incorporated radioactivity *Radiat Prot Dosimetry* **122** 521-7

Hoyes, Bingham, Hendry, Harrison, Sharma and Morris 1996 Transferrin-mediated uptake of plutonium by spermatogenic tubules *Int J Radiat Biol* **70** 467-71

Hoyes K P, Nettleton J S, Lawson R S and Morris I D 1998 Transferrin-dependent uptake and dosimetry of Auger-emitting diagnostic radionuclides in human spermatozoa *J Nucl Med* **39** 895-9

Hoyes K P, Sharma H L, Jackson H, Hendry J H and Morris I D 1994 Spermatogenic and mutagenic damage after paternal exposure to systemic indium-114m *Radiat Res* **139** 185-93

ICRP 1984 Nonstochastic Effects of Ionizing Radiation. ICRP Publication 41. *Ann ICRP* **14**

ICRP 2002 Basic anatomical and physiological data for use in radiological protection: reference values. ICRP Publication 89 *Ann ICRP* **32**

ICRP 2007 The 2007 Recommendations of the International Commission on Radiological Protection. ICRP publication 103 *Ann ICRP* **37**

ICRU 1984 Stopping Powers for Electrons and Positrons (Report 37) *Journal of the ICRU* **37**

ICRU 2002 International Commission on Radiation and Units. Absorbed-Dose Specification in Nuclear Medicine (Report 67) *Journal of the ICRU* **2** 1-110

Jackson C, Jackson H, Bock M, Morris I D and Sharma H L 1991 Metal radionuclides and the testis *Int J Rad Biol* **60** 851-8

Jönsson B-A, Andersson L and Strand S-E 1992a Biodistribution and Absorbed Doses of 111In-Labelled F(ab')2 Fragments Evaluated in Rats *Journal of Nuclear Medicine* **33** 1654-60

Jönsson B-A, Strand S-E, Emanuelsson H and Larsson B 1992b *Biophysical Aspects of Auger Processes, AAPM Symposium Series No. 8,* (Woodbury, NY: American Institute of Physics) pp 249-72

Jönsson B-A, Strand S-E and Larsson B 1992c A quantitative autoradiographic study of heterogenous activity distribution for different 111In-labeled radiopharmaceuticals in rat tissues *J Nucl Med* **33** 1825-33

Jönsson L, Liu X, Jönsson B-A, Ljungberg M and Strand S-E 2002 A dosimetry model for the small intestine incorporating intestinal wall activity and cross-doses *J Nucl Med* **43** 1657-64

Larsson E, Jonsson B A, Jonsson L, Ljungberg M and Strand S E 2005 Dosimetry calculations on a tissue level by using the MCNP4c2 Monte Carlo code *Cancer Biotherapy and Radiopharmaceuticals* **20** 85-91

Larsson E, Meerkhan S A, Strand S-E and Jönsson B-A 2012 A Small-Scale Anatomic Model for Testicular Radiation Dosimetry for Radionuclides Localized in the Human Testes *Journal of Nuclear Medicine* **53** 72-81

Loevinger R and Berman M 1976 *A revised schema for calculation of the absorbed dose from biologically distributed radionuclides. MIRD Phamplet No. 1, Revised* (New York: Society of Nuclear Medcine)

Meistrich M L 1986 Critical components of testicular function and sensitivity to disruption *Biol Reprod* **34** 17-28

Nettleton J S, Lawson R S, Prescott M C and Morris I D 2004 Uptake, localization, and dosimetry of In-111 and Tl-201 in human testes *J Nucl Med* **45** 138-46

Nickel M, Strand S E, Linden O, Wingardh K, Tennwall J and Gleisner K S 2009 Development and Evaluation of a Pharmacokinetic Model for Prediction of Radioimmunotherapy Based on Pretherapy Data *Cancer Biotherapy and Radiopharmaceuticals* **24** 111-21

Press W H, Teukolsky S A, Vetterling W T and Flannery B P 1992 *Numerical Recipes in Fortran,* (Cambridge: Cambridge University Press) pp 708-15

Rao D V, Govelitz G F and Sastry K S 1983 Radiotoxicity of thallium-201 in mouse testes: inadequacy of conventional dosimetry *J Nucl Med* **24** 145-53

Sgouros G and Hobbs R F 2014 Dosimetry for Radiopharmaceutical Therapy *Seminars in Nuclear Medicine* **44** 172-8

Sgouros G, Howell R W, Bolch W E and Fisher D R 2009 MIRD Commentary: Proposed Name for a Dosimetry Unit Applicable to Deterministic Biological Effects-The Barendsen (Bd) *Journal of Nuclear Medicine* **50** 485-7

Shen S, Meredith R, Duan J, Forero A, Breitz H, Khazaeli M B, Brezovich I and LoBuglio A 2005 Testicular uptake and radiation dose in patients receiving Zevalin and Pretarget CC49Fusion protein *Cancer Biother Radiopharm* **20** 110-8

Sjögreen K, Ljungberg M, Wingardh K, Minarik D and Strand S E 2005 The LundADose method for planar image activity quantification and absorbed-dose assessment in radionuclide therapy *Cancer Biotherapy and Radiopharmaceuticals* **20** 92-7

Sjögreen-Gleisner K 2012 Scatter correction by deconvolution of planar whole-body scintillation-camera images using an image-based estimate of the signal-to-noise ratio *European Journal of Nuclear Medicine* **39** S304-S53

Sjögreen-Gleisner K, Dewaraja Y K, Chiesa C, Tennvall J, Linden O, Strand S E and Ljungberg M 2011 Dosimetry in patients with B-cell lymphoma treated with Y-90 ibritumomab tiuxetan or I-131 tositumomab *Q. J. Nucl. Med. Mol. Imag.* **55** 126-54

Sjögreen-Gleisner K and Ljungberg M 2012 Patient-specific whole-body attenuation correction maps from a CT system for conjugate-view-based activity quantification: method development and evaluation *Cancer Biother Radiopharm* **27** 652-64

Sjögreen-Gleisner K, Nickel M, Lindén O, Erlandsson K, Wingårdh K and Strand S-E 2007 Parametric Images of Antibody Pharmacokinetics Based on Serial Quantitative Whole-Body Imaging and Blood Sampling *Journal of Nuclear Medicine* **48** 1369-78

Stenvall A, Larsson E, Strand S E and Jonsson B A 2014 A small-scale anatomical dosimetry model of the liver *Phys Med Biol* **59** 3353-71

Tennvall J, Fischer M, Bischof Delaloye A, Bombardieri E, Bodei L, Giammarile F, Lassmann M, Oyen W and Brans B 2007 EANM procedure guideline for radio-immunotherapy for B-cell lymphoma with 90Y-radiolabelled ibritumomab tiuxetan (Zevalin) *Eur J Nucl Med Mol Imaging* **34** 616-22

Wiseman G A, Leigh B R, Dunn W L, Stabin M G and White C A 2003a Additional radiation absorbed dose estimates for Zevalin (TM) radioimmunotherapy *Cancer Biotherapy and Radiopharmaceuticals* **18** 253-8

Wiseman G A, Leigh B R, Erwin W D, Sparks R B, Podoloff D A, Schilder R J, Bartlett N L, Spies S M, Grillo-Lopez A J, Witzig T E and White C A 2003b Radiation dosimetry results from a Phase II trial of ibritumomab tiuxetan (Zevalin) radioimmunotherapy for patients with non-Hodgkin's lymphoma and mild thrombocytopenia *Cancer Biother Radiopharm* **18** 165-78

Yousif L, Blettner M, Hammer G, amp, l P and Zeeb H 2010 REVIEW Testicular cancer risk associated with occupational radiation exposure: a systematic literature review *J Radiol Prot* **30** 389-406